BULLETIN OF THE POLISH ACADEMY OF SCIENCES
TECHNICAL SCIENCES, Vol. 73(5), 2025, Article number: e154202
DOI: 10.24425/bpasts.2025.154202

Numerical simulation of transient startup characteristics in pump-driven two-phase flow systems

Nianyong ZHOU*, Jing LI, Jixiang LIU, Kaiming LIU, Feifei WANG, and Lianghui LIU

School of Urban Construction, Changzhou University, Changzhou, China

Abstract. The pump-driven two-phase flow system is widely used in electronic cooling due to its high heat transfer efficiency and stable temperature control. However, transient startup behaviors, crucial for reliability in dynamic thermal environments, remain poorly understood. This study addresses this gap by developing a simulation model using AMESim software with R134a as the working fluid, investigating the effects of heat load, pump speed and cooling water temperature on startup dynamics. Results reveal three distinct startup types: Type I rising startup, Type II rising startup, and Type I falling startup. As the heat load increases from 2 kW to 5 kW, the system transitions from Type I to Type II, with the cold plate wall temperature decreasing by up to 27%. At 2 kW and 5 kW, the system exhibits Type I upward and Type II upward startup behaviors, respectively. Type II startup demonstrates reduced overshoot, enabling quicker approach to quasi-steady state. At 2 kW, the system exhibits both single-phase and two-phase heat transfer, with the latter lowering the temperature by 2.26°C. Excessive subcooling can induce temperature oscillations within the evaporator. At a pump speed of 200 r/min, Type I upward startup is observed; however, increased speeds result in wall temperature overshoot. Furthermore, raising the cooling medium temperature from 10°C to 40°C elevates the evaporator wall temperature by 51.67%. By integrating quantitative metrics for overshoot, response time and subcooling effects, this work provides actionable insights for optimizing pump-driven two-phase systems in high-heat-flux electronic cooling applications.

Keywords: pump; two-phase flow; heat transfer; evaporative cold plate; startup characteristics.

NOMENCLATURE

Symbols

$carea$	convective exchange surface, mm^2
c_p	specific heat capacity, $J{\cdot}kg^{-1}K^{-1}$
Dh	hydraulic diameter, mm
E	total amount of received work, J
h	heat transfer coefficient, $Wm^{-2}K^{-1}$,
m	mass flow rates, kgs^{-1},
n	pump speed, r/min
Nu	Nusselt number
P	pressure, Pa
Pr	Prandtl number
Q	cumulative rate of heat flow
Re	Reynolds number
t	time, s
T	temperature, °C
U	internal energy, J
x	quality
X	vapor quality

Subscripts

c	cooling medium
cr	critical
cv	forced convection
$disp$	displacement of the pump
i	inlet
LF	liquid flow
lam	laminar
ncb	contribution of nucleate boiling
suc	suction
$turb$	turbulence
v	volume
vol	volume of the fluid, m^3

Greek symbols

η	pump efficiency
ξ	drag coefficient
ρ	fluid density, kgm^{-3}
λ	thermal conductivity

1. INTRODUCTION

The enhancement of the integration and miniaturization of electronic devices has led to a continuous increase in thermal load and heat flux [1, 2]. However, traditional cooling methods such as air cooling [3] and liquid cooling [4] pose problems such as

*e-mail: zhounianyong@cczu.edu.cn

Manuscript submitted 2025-01-14, revised 2025-02-28, initially accepted for publication 2025-03-10, published in July 2025.

limited heat exchange capacity, low efficiency and large volume, and thus cannot meet the heat dissipation requirements. If the heat cannot be dissipated in a timely manner, it may cause overheating of electronic devices, resulting in impaired reliability and even irreversible damage [5, 6].

Currently, the cooling methods for high heat flux density electronic devices include jet impingement technology [7], spray cooling technology [8], and pump-driven two-phase flow cooling technology [9]. Jet cooling has a large heat transfer coefficient in the impingement area. However, in most areas other than the impingement area, heat transfer performance decreases rapidly as it spreads to the surroundings, forming a large temperature gradient, which may cause failure of some temperature-sensitive devices. Spray cooling atomizes the pressure flow into small droplets through a nozzle and sprays them onto the surface of avionics equipment for heat dissipation. It offers the advantages of strong heat transfer capacity, small coolant flow rate and high critical heat flux. However, its heat transfer mechanism is complex, and the pressure of the nozzle is relatively high, making it prone to unreliable problems. Pump-driven two-phase flow cooling is an emerging active thermal control cooling technology, which exhibits great development potential in the field of electronic heat dissipation. This cooling technology relies on the vaporization and condensation of the working medium throughout the process to complete the absorption, transportation and dissipation of the heat generated by electronic devices.

Pump-driven two-phase flow cooling technology is applied to electronic devices with high heat flux density. In 2014, NASA presented the research results, indicating that the micro-pumped cooling loop (MPCL) is highly suitable for high heat flux density heat dissipation because it has many advantages in terms of high heat transfer rate, long-distance heat transfer capability and precise temperature control.

Huang *et al*. [10] analyzed the MPCL circuit and reservoir branches applied to the Alpha Magnetic Spectrometer-02 (AMS-02), and proposed that the operating temperature of the system could be controlled by regulating the temperature of the working medium in the reservoir. Experiments and simulations showed that fluctuations in the ambient temperature on the condenser side and the heat load on the evaporator side would cause fluctuations in the temperature of the working medium in the reservoir, which in turn would lead to fluctuations in the operating temperature of the loop. Meng *et al*. [11] developed a temperature-controlled liquid reservoir for MPCL, aiming to meet the strict requirements of the core components of spacecraft for precise and stable temperature control. The experimental results demonstrated that this reservoir has the advantages of simple design, low power consumption and high reliability, and it meets the requirements of temperature regulation. Wang *et al*. [12] proved through experiments that MPCL exhibits excellent performance in both steady-state heat transfer and transient stability, making it highly suitable for thermal management applications in avionics equipment.

Current research on pump-driven two-phase flow cooling systems focuses primarily on maximizing heat dissipation capacity, improving temperature control accuracy, and enhancing temperature uniformity. Through experimental investigations, Mudawar *et al*. [13, 14] developed a microchannel evaporative cold plate demonstrating an exceptional heat transfer coefficient of 840 W/cm^2. Additionally, Wang *et al*. [15] experimentally demonstrated that microchannel evaporative cold plates with sudden contraction inlets exhibit enhanced stability. Schweizer *et al*. [16] proposed a novel concept of a miniature pump-driven two-phase flow loop, and systematically investigated its thermal performance and stability characteristics. Their experimental results demonstrated a significant enhancement in heat transfer capability. Wang *et al*. [17] implemented a liquid reservoir to regulate the system's evaporation temperature, achieving precise temperature control within ±0.5°C for the evaporative cold plate. Bejarano *et al*. [18] developed a gas-liquid separation evaporator integrated with a proportional-integral (PI) control algorithm to optimize boiling conditions, effectively mitigating temperature and pressure surges during system startup. Crepinsek [19] designed a dual-evaporator two-phase cooling system and conducted comparative studies under series and parallel configurations. Experimental results demonstrated that the parallel configuration significantly enhanced heat transfer capacity while maintaining superior temperature uniformity in the evaporators. Ambrose *et al*. [20] implemented a bypass circuit to deliver two-phase working fluid from the evaporator to the pump inlet, demonstrating stable system operation and adaptability across various working conditions. Pereira *et al*. [21] investigated the optimal refrigerant charge using R134a and R1234yf as working fluids, employing eight distinct predictive models with mean relative errors of 12% and 13%, respectively.

Regarding dynamic characteristics, Jiang *et al*. [22] designed an impeller pump to investigate the transient behavior of a mechanically pumped cooling loop (MPCL), using methanol as the working fluid. Their findings demonstrated that the preset conditions of the evaporator significantly influence the startup characteristics. The two-phase mechanically pumped loop (TMPL) offers distinct advantages for thermal management, including extended heat transfer distance, high thermal density and precise temperature control. Understanding the fluid charge quantity is crucial for optimizing TMPL system efficiency. Meng *et al*. [23] examined the transient behavior of MPCL during thermal load application/removal, observing that both temperature and pressure in the accumulator required two oscillations to regain stability. Notably, the fluctuation patterns between these two processes exhibited opposite trends. Additionally, reducing pump speed resulted in decreased stable temperature, flow resistance, and mass flow rate within the evaporator. Deng *et al*. [24] conducted an in-depth investigation into the effects of step thermal loads on evaporator startup performance in MPCL. Their study revealed that as the step thermal load progressively increased, the evaporator sequentially exhibited gradual startup, first overshoot initiation, and secondary overshoot initiation. The observed temperature overshoot was primarily attributed to boiling initiation. Wang *et al*. [25] developed a paraffin-driven adaptive thermal control valve to regulate the heat dissipation capacity of evaporative cold plates under dynamic thermal loads, demonstrating that the temperature fluctuation of the heat source remained within the range of 34 ± 2°C.

Based on a comprehensive literature review, overcoming startup challenges is a critical prerequisite for the reliable operation of pump-driven two-phase cooling systems, where rapid thermal response serves as a key performance indicator during both system initialization and step thermal load variations. Given the limited research on startup characteristics and insufficient consideration of influencing factors, this study employs an integrated approach combining theoretical analysis and system simulation. Initially, a pump-driven two-phase cooling system was constructed, followed by the development of a comprehensive simulation model using AMESim software to investigate the transient startup characteristics. This study systematically examines the influence of various factors on system performance and provides quantitative insights into overshoot and response time, offering theoretical insights and empirical data to support performance enhancement and optimization of pump-driven two-phase flow systems.

2. MODELING AND VERIFICATION OF PUMP-DRIVEN TWO-PHASE FLOW SYSTEMS

2.1. System principles

Figure 1 shows the schematic outline of the pump-driven two-phase flow system, which consists of a mechanical pump, evaporator, condenser, liquid reservoir, preheater, filter and piping.

(a) experimental platform

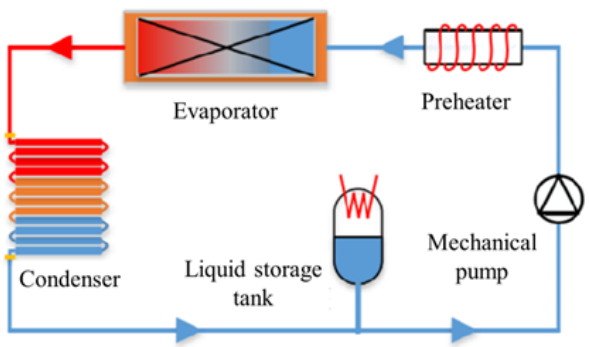

(b) schematic diagram

Fig. 1. Pump-driven two-phase flow cooling system setup and diagram

The system operates as follows: the circulation pump draws subcooled working fluid from the reservoir, passing it through the mechanical pump and preheater for initial heating. After reaching a saturated state, the fluid enters the evaporator, exchanges heat with the heat source, and undergoes a phase change. The high-temperature fluid, in both gas and liquid phases, returns to the condenser to release heat via condensation before flowing back to the liquid reservoir, thus completing a closed loop.

To investigate the heat transfer mechanism of the pump-driven two-phase flow system, a simplified model of the system was established based on the following fundamental assumptions: the working fluid exhibits one-dimensional flow within the evaporator; under two-phase flow conditions, the working fluid is considered to be in thermodynamic equilibrium and is treated as a homogeneous flow; the evaporator model focuses solely on the flow path of the working fluid, disregarding heat exchange between the cold plate and the surrounding air.

2.2. Modeling of the system

In this model, R134a is selected as the working fluid. The dynamic characteristics of the system are analyzed to explore the variations of the fluid parameters under various operating conditions. All thermophysical parameters are derived by utilizing a two-phase flow library at each time step.

A two-phase flow pump with a displacement of 20 cm^3 is employed, with its rotational speed controlled by a signal source, enabling the adjustment of the working fluid flow rate. The pump exhibits a volumetric efficiency of 0.5, an isentropic efficiency of 0.65, and a mechanical efficiency of 0.7.

Volumetric efficiency is utilized to determine the mass flow rate at the outlet of the two-phase flow pump, as illustrated below:

$$dm_2 = \eta_v \cdot \rho_{suc} \cdot N \cdot disp. \tag{1}$$

The evaporator is configured as an evaporative cold plate, with the parameters of the fins and the heat exchange between the cold plate and the surrounding air being disregarded. A two-phase flow pipeline is employed for simulation alongside a thermal mass block, with all initial parameters specified. The two-phase flow pipeline is initially set at a pressure of 20 bar and a temperature of 70°C. The thermal mass block had an initial temperature of 70°C, made of aluminum. The single channel of the evaporative cold plate is segmented into four components, each 52.5 mm long, and interconnected through a generic conduction component. These components are arranged in a grid format, consisting of 78 rows and 4 columns. Figure 2a illustrates the partial evaporator model. Each thermal mass block is connected to a two-phase flow pipe for calculating the heat removed by the working fluid through the cold plate, while neglecting heat exchange between the cold plate and ambient air. Although the evaporator contains both subcooled and evaporative regions, identical refrigerant energy balance is maintained for each control volume under constant heat flux conditions, as schematically shown in Fig. 2b.

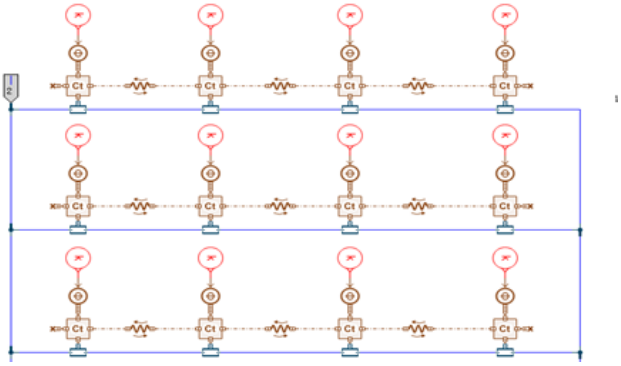

(a) partial evaporator model

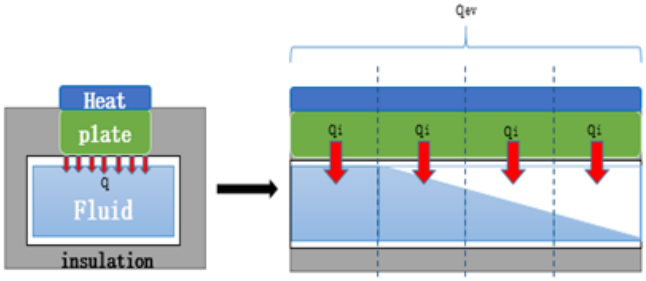

(b) schematic diagram

Fig. 2. Evaporative cold plate model diagram

The temperature variation of the cold plate is calculated by adjusting the thermal mass parameters.

$$\frac{\mathrm{d}T}{\mathrm{d}t} = \frac{\sum_{i=1}^{4} dh_i}{mass \cdot c_p}. \tag{2}$$

The heat transfer rate of the two-phase flow pipe can be determined by calculating the convective heat transfer between the two-phase flow pipe and the thermal mass block, as shown below:

$$dmh_2 = h \cdot carea \cdot (T_1 - T_2) \cdot dhgn. \tag{3}$$

The time derivative of density in a control volume is derived from the principle of mass conservation and is represented as follows:

$$\frac{\mathrm{d}\rho}{\mathrm{d}t} = \frac{1}{vol} \cdot \sum \dot{m}_i. \tag{4}$$

The derivative expression of pressure with respect to time is derived from the principle of conservation of volumetric energy, as expressed below:

$$\frac{\mathrm{d}U}{\mathrm{d}t} = \dot{E} + \sum \dot{m} \cdot h_i + \dot{Q}. \tag{5}$$

The equation is reformulated as a function of the time derivative of temperature (used here for intermediate calculations) and the time derivative of density, expressed as follows:

$$\frac{\mathrm{d}T}{\mathrm{d}t} = \frac{1}{m \cdot cv} \cdot \begin{pmatrix} \sum \dot{m}_i \cdot h_i + \dot{Q} - h \cdot \sum \dot{m}_i \\ -m \cdot \left(P + \left.\frac{\partial u}{\partial v}\right|_T \right) \cdot \frac{\mathrm{d}v}{\mathrm{d}t} \end{pmatrix}. \tag{6}$$

The condenser model employs a plate-type condenser, where the initial pressure of the refrigerant side is set at 3 bar, and the initial pressure of the cooling water side is maintained at standard atmospheric pressure. The coolant used is water.

The preheater utilized a thermoelectric capacitor and constant thermal current simulation, allowing for real-time adjustment of thermal power. By altering the signal source parameters, the thermal power of the heat source can be adjusted. The initial pressure of the storage tank is established at 8 bar, with an initial liquid volume fraction of 50% and a total volume of $1.2L$.

Universal sensors are positioned at the inlet and outlet of the storage tank, evaporator, condenser and pump in order to monitor changes in parameters such as temperature and pressure throughout the simulation process. The complete system model is presented in Fig. 3.

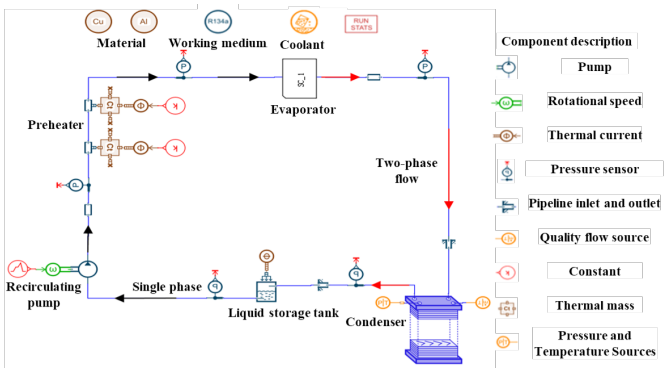

Fig. 3. Pump-driven two-phase flow system model

2.3. Heat transfer process analysis

The evaporator and condenser models concentrate exclusively on the heat transfer occurring on the refrigerant side (internal flow) and the solid wall surfaces. Given the presence of various operating conditions, such as subcooling and superheating, the internal heat transfer consists of both single-phase and two-phase regions.

In the case of laminar single-phase flow, the convective heat transfer coefficient is defined as follows:

$$h_{lam} = \mathrm{Nu}_{lam} \cdot \frac{\lambda}{Dh}. \tag{7}$$

For turbulent single-phase flow, the convective heat transfer coefficient can be determined using the Gnielinski correlation [18] as follows:

$$h_{turb} = \frac{\left(\frac{\xi}{8}\right) \cdot [\mathrm{Re} - 1000] \cdot \mathrm{Pr}}{1 + 12.7\sqrt{\frac{\xi}{8}} \cdot \left[\mathrm{Pr}^{2/3} - 1.0\right]} \cdot \frac{\lambda}{Dh}. \tag{8}$$

Condensation occurs when the refrigerant temperature surpasses the temperature of the inner wall of the condenser. The heat transfer in the two-phase region of the condenser is described using the Shah correlation [26, 27], as represented by the following:

$$h_{TP} = h_{LF}\left[(1-x)^{0.8} + \left(3.8 \cdot \frac{x^{0.76}(1-x)^{0.04}}{\left(\frac{P}{P_{cr}}\right)^{0.38}}\right)\right], \quad (9)$$

$$h_{LF} = 0.023 \cdot \mathrm{Re}_{LF}^{0.8} \cdot \mathrm{Pr}^{0.3} \cdot \frac{\lambda_l}{Dh}. \quad (10)$$

The phenomenon occurring in the evaporator tubes involves the evaporation phase change process, which is contrary to the condensation process. By employing the VDI (horizontal tube) experimental correlation [28], the heat transfer coefficient for the two-phase flow can be formulated as follows:

$$h = \sqrt[3]{h_{cv}^3 + h_{ncb}^3}. \quad (11)$$

2.4. Model reliability verification

The specific steps of the experiment are as follows:

1. Start the condensing chiller and pre cooling chiller to subcool the refrigerant at the pump inlet.
2. When the temperature of the refrigeration circuit is lower than the ambient temperature, start the gear pump and adjust the flow rate.
3. Activate the DC power supply and set the voltage to achieve the desired power (or heat flux density). As the heating element's resistance varies with voltage, iterative adjustments are required to align the actual power with the target value.
4. Set the condensing chiller temperature to the target value. For airborne applications, maintain identical temperatures for both pre-cooling and condensing chillers.
5. Adjust the micro regulating valve to bring the system pressure to the set value.
6. When the experimental conditions are reached and the system is stable, collect experimental data. Record at a frequency of once per second for at least 60 seconds at each operating point.
7. After the experiment, turn off the heating power, pump power and chiller power in sequence.
8. Repeat the above steps until all operating conditions are completed.

Model reliability analysis is effected through error assessment of simulation and experimental results. The experimental conditions were established with saturation pressure P = 0.5 MPa, cooling water temperature T_c = 5°C, mass flow rate of 100 kg/(m^2·s), thermal load Q = 882 W, and heat flux density q = 30 kW/m^2. The results are presented in Fig. 4, where the x-axis represents vapor quality (X) and the y-axis corresponds to heat flux density (h). The experimental and simulated results exhibit similar trends, with maximum error of 7%, meeting engineering calculation requirements. Therefore, studying pump-driven two-phase flow heat transfer characteristics based on the AMESim model is feasible.

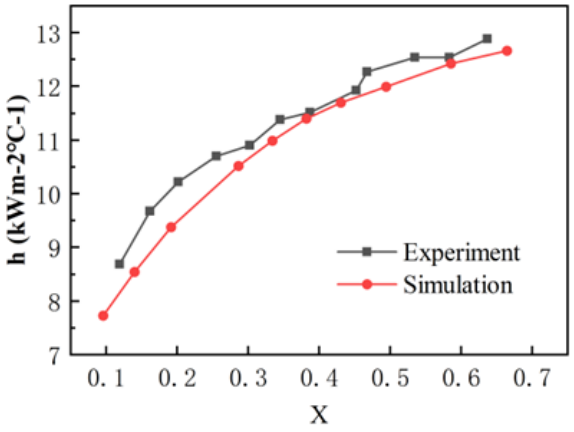

Fig. 4. Comparison of model and test results

3. RESULTS AND ANALYSIS

3.1. Impact of startup under stepwise thermal loads

The startup characteristics of a pump-driven two-phase flow cooling system involve a complex interplay of processes, including heat conduction at the evaporative cooling plate wall, internal gas-liquid two-phase flow within the cooling plate, and nucleate boiling of the fluid. Based on the dynamic temperature change curves of the evaporative cooling plate and condenser, the startup types can be categorized into Type I rising startup, Type II rising startup and Type I falling startup. The dynamic temperature change curves of the evaporative cooling plate wall for each corresponding startup type are presented in Fig. 5.

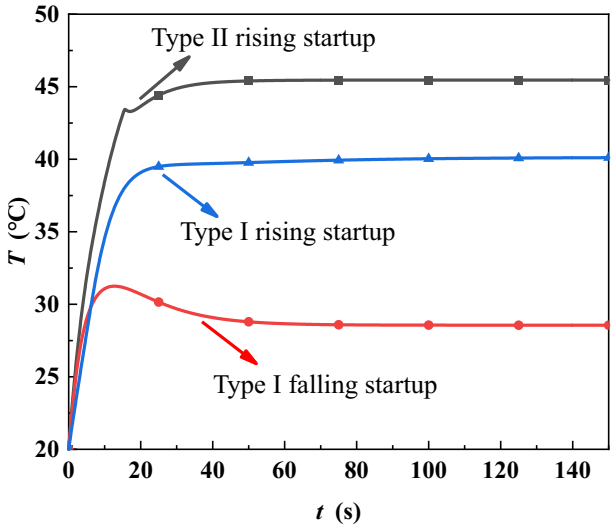

Fig. 5. Schematic representation of various startup types

The circulation pump operates at a speed of 1000 r/min, with the cooling medium temperature maintained at 30°C during the startup phase. Figure 6 presents the wall temperature variation of the evaporative cooling plate with thermal load. The data reveal that the surface temperature trends of the evaporative cooling plate vary significantly with the changes in thermal load, indicating a transition in the system's startup type. Furthermore,

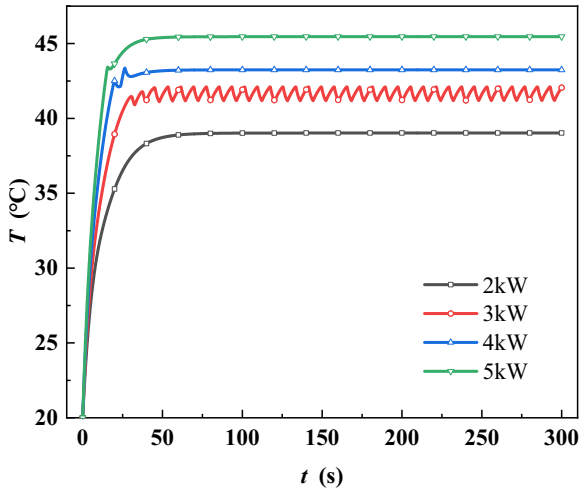

Fig. 6. Wall temperature variation of the evaporative cooling plate with thermal load

as the thermal load increases, the response time of the evaporative cooling plate decreases, and the system's overshoot also reduces, facilitating faster approach to a quasi-steady state.

During system startup, when the external thermal load on the evaporative cold plate was 2 kW, the wall temperature of the cold plate rose sharply at first, then increased gradually, ultimately approaching a quasi-steady state. Throughout the entire startup process, wall temperature exhibited a monotonic increase, characteristic of at the Type I rising startup. When the thermal load reached 3 kW, wall temperature experienced slight oscillations, indicating that phase change began to occur at the inlet of the evaporative cold plate. The onset of two-phase flow caused variations in inlet temperature, resulting in an overshoot in wall temperature.

Moreover, at external thermal loads of 4 kW and 5 kW, the oscillation amplitude of the wall temperature decreases progressively, and the transition from one-phase flow to two-phase flow becomes increasingly gradual. As the fluid flows in the designated direction, the temperature oscillations of the evaporative cooling plate evolve into a quasi-steady state. At a thermal load of 5 kW, the startup behavior of the evaporative cooling plate is identified as a Type II rising startup.

Figure 7 presents the parameter variation in the evaporative cooling plate at 2 kW along flow direction. As depicted in Fig. 7a, at 52.5 mm along the flow direction within the evaporative cold plate, the working fluid was in a single-phase state. As it flowed toward the outlet, the dryness increased, and the phase change became more pronounced near the outlet; however, this phase change had little effect on the wall temperature. Figure 7b indicates that at the inlet of the evaporative cold plate, wall temperature reaches 39.02°C during single-phase heat transfer of the working fluid. The temperature gradually decreases along the flow direction, reaching a minimum of 36.76°C at the outlet. At the last three observation points, the working fluid is in a two-phase state, which significantly enhances heat transfer performance. Consequently, in the Type I rising startup process, the working fluid initially operates in a single-phase flow state. As thermal load is applied, wall temperature gradually

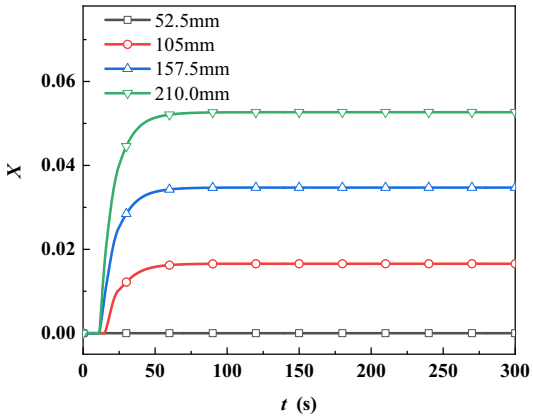

(a) change in dryness of working fluid

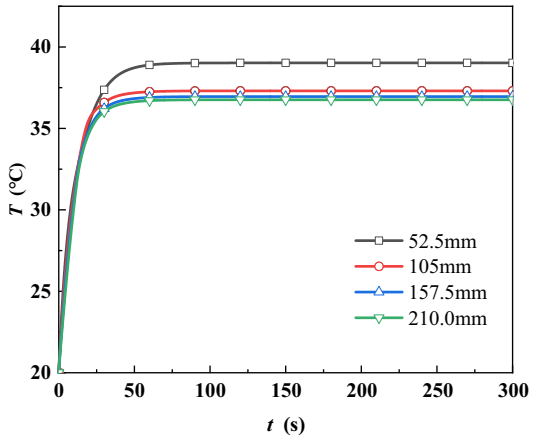

(b) wall temperature variation

Fig. 7. Parameter variation in the evaporative cooling plate at 2 kW along flow direction

increases. When wall temperature exceeds the saturation temperature and reaches a certain degree of superheat, the working fluid gradually undergoes a phase change, leading to the formation of bubbles in the vapor core. As the external thermal load continues to increase, heat transfer becomes more intense, eventually transitioning to nucleate boiling heat transfer. This process marks the shift of the working fluid from single-phase flow to two-phase flow heat transfer.

The evaporative cooling plate is initially set to a pressure of 8 bar, with the working fluid starting at a temperature of 31.3°C and the ambient temperature at 20°C. Figure 8 shows the wall temperature variations of the evaporative cooling plate under a thermal load of 5 kW. This startup type includes the initial temperature rise phase, the temperature overshoot decrease phase, the continued temperature rise phase and the quasi-steady state phase.

Figure 8 shows that during the initial phase, as the evaporative cold plate's wall temperature rises, the working fluid remains in a subcooled state, absorbing heat for single-phase heat transfer. When wall temperature experiences an overshoot and decreases, nucleate boiling occurs in the channel, altering the heat transfer mechanism and causing a rapid decline in wall tem-

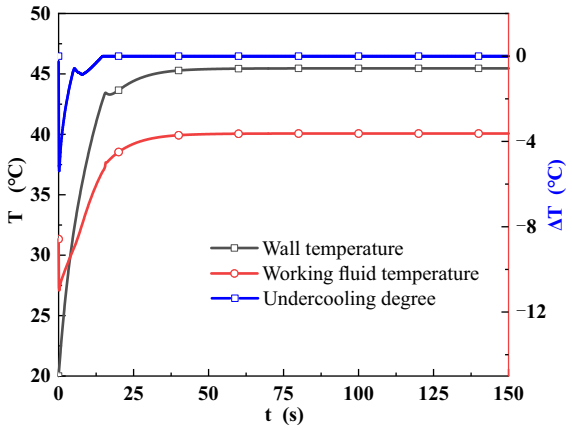

Fig. 8. Parameter variations in the evaporative cooling plate at 5 kW thermal load

perature. As the temperature continues to rise, the heat transfer mechanism shifts again, transitioning the two-phase fluid from nucleate boiling to convective evaporation heat transfer, thereby enhancing its performance. Once the wall temperature reaches a quasi-steady state, the temperature of the phase-changed fluid remains relatively constant, with its latent heat sufficiently carrying away the external thermal load and maintaining a stable wall temperature. For example, with an external thermal load of 5 kW, the inlet temperature of the subcooled fluid is 40.07°C, while the outlet temperature is 39.88°C, resulting in a minimal temperature difference of 0.19°C.

3.2. Startup characteristics with varying pump rotational speeds

The rotational speed of the circulation pump directly determines the mass flow rate of the working fluid. As the circulation pump speed increases, the working fluid flow rate correspondingly rises. Under constant external conditions, this requires greater heat input for phase transition. The system necessitates higher wall temperatures to initiate vapor bubble formation and provide the requisite disturbance energy for phase change. This thermal perturbation facilitates the transition to two-phase flow. Once established, the two-phase flow significantly enhances the heat transfer coefficient, leading to gradual wall temperature reduction. The gas-liquid mixture continues with its heat exchange, and under sustained external thermal load, the wall temperature stabilizes into a quasi-steady state. This section investigates the startup characteristics under varying pump speeds with an external thermal load of 4 kW and a cooling medium temperature of 15°C. Figure 9 illustrates the transient variations in cold plate wall temperature at varying pump speeds.

From Fig. 9, it can be observed that as the pump speed continues to increase, the wall temperature exhibits a monotonic change followed by a downward trend. This decreasing trend is directly proportional to the pump speed. This type of startup is defined as Type I descending startup.

Figure 9a shows that at a pump speed of 200 r/min, the evaporative cold plate demonstrates the Type I rising startup. Due to the low mass flow rate, the working fluid rapidly transitions to

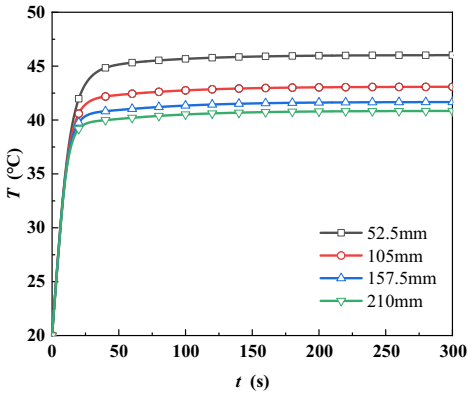

(a) n = 200 r/min

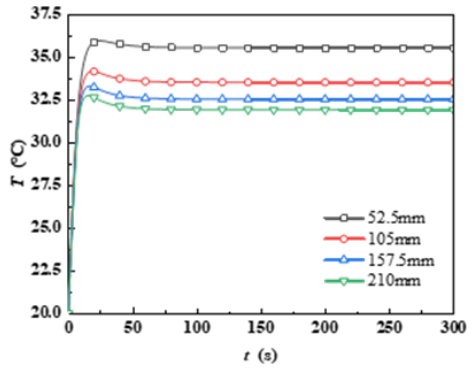

(b) n = 500 r/min

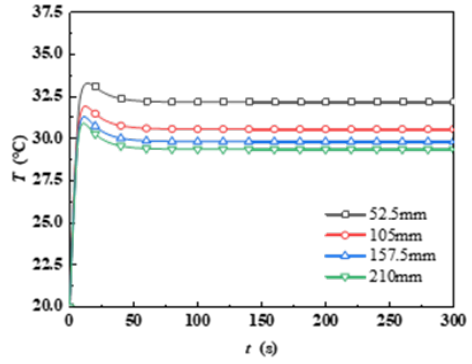

(c) n = 650 r/min

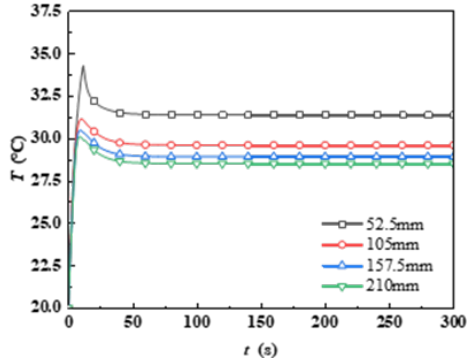

(d) n = 800 r/min

Fig. 9. Transient variations in cold plate wall temperature at varying pump speeds

two-phase flow upon entering the evaporative cold plate, resulting in the highest quality at the inlet among the four conditions, with a maximum wall temperature of 46.01°C. As the working fluid flows toward the outlet of the evaporative cold plate, the intensity of nucleate boiling heat transfer increases, leading to lower wall temperature.

Figure 9d observed that at a pump speed of 800 r/min, the working fluid initially undergoes single-phase heat transfer, resulting in a "spike". Due to the high fluid flow rate, a significant wall temperature disturbance is necessary for the transition from single-phase to two-phase flow. After the phase change of the working fluid, wall temperature experiences an overshoot and decreases, quickly reaching a quasi-steady state.

As shown in Fig. 9, with the increase in pump speed, the wall temperature consistently decreases; however, at excessively high pump speeds, an overshoot phenomenon occurs in the wall temperature. This phenomenon affects the uniformity of the wall temperature of the evaporative cold plate in an adverse manner, indicating that as the pump speed increases, the "spike" phenomenon emerges.

3.3. Startup characteristics at varying cooling medium temperatures

Figure 10 presents the dynamic variation curves of the evaporative cold plate wall temperature as a function of the condenser cooling medium temperature, under a thermal load of $Q = 4$ kW and a circulation pump speed of 1000 r/min, for four different cooling medium temperatures.

Figure 10 demonstrates that when the cooling water temperature increases from 10°C to 40°C, the wall temperature of the evaporative cold plate rises by 51.67%. The wall temperature curves for different cooling media initially exhibit a monotonic increase, followed by varying characteristics corresponding to different startup types, and eventually reaching a quasi-steady state. After reaching a quasi-steady state, wall temperatures decrease due to the lowered cooling medium temperature, which results in reduced temperatures of all components in the system. The two-phase fluid, upon condensation, becomes a subcooled liquid before re-entering the evaporative cold plate, further lowering its temperature and requiring additional heat to achieve saturation.

At cooling medium temperatures of 10°C, 20°C, 30°C and 40°C, the supercooling at the inlet of the evaporative cold plate is 5.79°C, 4.16°C, 2.93°C and 1.46°C, respectively, indicating that a significant amount of heat must be absorbed to reach saturation. As shown in Fig. 10, wall temperature startup types at the inlet of the cold plate are the Type I falling startup for 10°C, the Type I rising startup for 20°C, the Type II rising startup for 30°C, and the Type I rising startup for 40°C. As the cooling medium temperature decreases, the startup type of the wall temperature changes accordingly, leading to an increase in the supercooling at the working fluid inlet. This change affects the occurrence of wall temperature overshoot; the greater the supercooling, the earlier the transition of the working fluid within the evaporative cold plate to a two-phase flow due to overshoot. However, a larger temperature difference at the wall results in poorer uniformity of the wall temperature.

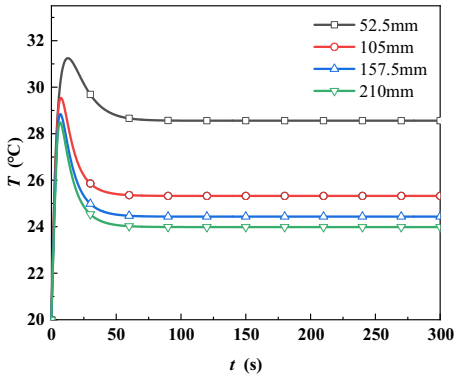

(a) $T_c = 10$°C

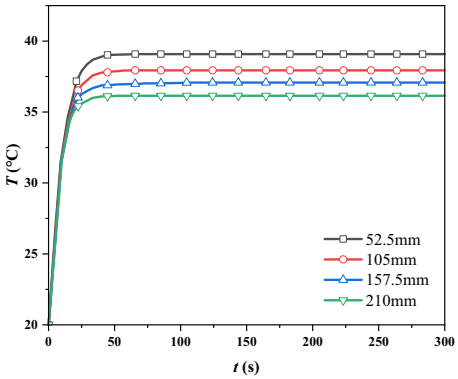

(b) $T_c = 20$°C

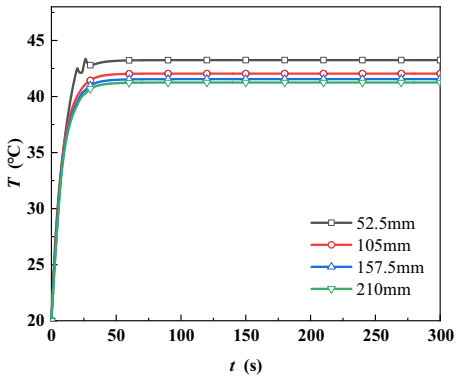

(c) $T_c = 30$°C

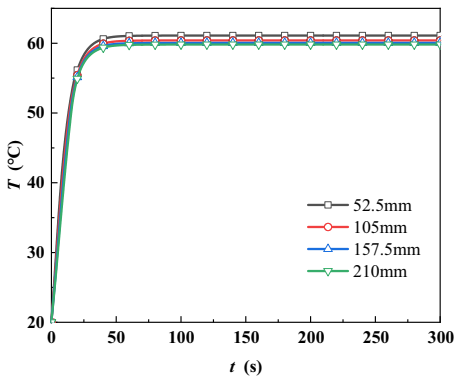

(d) $T_c = 40$°C

Fig. 10. Wall temperature of the evaporative cold plate at different cooling medium temperatures

4. CONCLUSIONS

This study establishes a mathematical model for a pump-driven two-phase flow cooling system, and conducts numerical simulations to evaluate its dynamic performance. The research systematically investigates the effects of step thermal loads, circulation pump speed and cooling medium temperature on transient startup characteristics. The key findings, which are applicable to a wide range of thermal management systems, are summarized as follows:

1. The transient startup characteristics of pump-driven two-phase flow systems can be universally categorized into three distinct types: Type I monotonic rising, Type I descending and Type II stabilized rising. These behaviors are governed by the interplay of thermal load thresholds and operational parameters. As the thermal load increases, the system transitions from Type I to Type II startup, which is a process characterized by reduced overshoot and accelerated stabilization.
2. As the pump speed increases, the startup characteristics of the system transition from Type I monotonic rising to Type I descending. At higher pump speeds, a pronounced "spike" phenomenon emerges, resulting in significant wall temperature overshoot and degraded spatial uniformity. This behavior is universally observed in two-phase flow systems, where elevated flow rates require greater thermal perturbation to initiate phase change, leading to transient instability.
3. The transient startup characteristics of the system are significantly influenced by the cooling medium temperature. As the cooling medium temperature decreases, the system exhibits sequential transition in startup behavior, progressing from Type I descending to Type II ascending and finally to Type I ascending. This transition is primarily driven by the reduction in subcooling at higher cooling medium temperatures, which shifts the system from a pure liquid phase to a gas-liquid two-phase flow at the thermal exchange outlet.

REFERENCES

[1] I. Afaynou, H. Faraji, K. Choukairy, A. Arshad, and M. Arıcı, "Heat transfer enhancement of phase-change materials (PCMs) based thermal management systems for electronic components: A review of recent advances," *Int. Commun. Heat Mass Transf.*, vol. 143, p. 106690, Apr. 2023, doi: 10.1016/ j.icheatmasstransfer.2023.106690.

[2] H.-C. Chiu, J.-H. Jang, H.-W. Yeh, and M.-S. Wu, "The heat transfer characteristics of liquid cooling heatsink containing microchannels," *Int. J. Heat Mass Transf.*, vol. 54, no. 1, pp. 34–42, Jan. 2011, doi: 10.1016/j.ijheatmasstransfer.2010.09.066.

[3] T. Chenqi, Y. Zhongjun, F. Jia, Y. Juntan, and J. Hao, "Temperature field analysis of an air-water composite cooling high-speed generator," *Case Stud. Therm. Eng.*, vol. 65, p. 105646, Jan. 2025, doi: 10.1016/j.csite.2024.105646.

[4] C. Liu, M. Li, D. Hu, Y. Zheng, L. Cao, and Z. He, "Liquid Metal-Enabled Synergetic Cooling and Charging of Superhigh Current," *Engineering*, Dec. 2024, doi: 10.1016/j.eng.2024.11.035.

[5] X. Huo, L. Chen, Y.S. Tian, and T.G. Karayiannis, "Flow boiling and flow regimes in small diameter tubes," *Appl. Therm. Eng.*, vol. 24, no. 8, pp. 1225–1239, Jun. 2004, doi: 10.1016/j.applthermaleng.2003.11.027.

[6] T. Chen and S. V. Garimella, "Measurements and high-speed visualizations of flow boiling of a dielectric fluid in a silicon microchannel heat sink," *Int. J. Multiphase Flow*, vol. 32, no. 8, pp. 957–971, Aug. 2006, doi: 10.1016/j.ijmultiphaseflow.2006.03.002.

[7] R. van Hout, V. Rinsky, and Y.G. Grobman, "Experimental study of a round jet impinging on a flat surface: Flow field and vortex characteristics in the wall jet," *Int. J. Heat Fluid Flow*, vol. 70, pp. 41–58, Apr. 2018, doi: 10.1016/j.ijheatfluidflow.2018.01.010.

[8] A. Sarmadian, J.F. Dunne, C.A. Long, J.T. Jose, J.-P. Pirault, and C. Rouaud, "Heat flux correlation models for spray evaporative cooling of vibrating surfaces in the nucleate boiling region," *Int. J. Heat Mass Transf.*, vol. 160, p. 120159, Oct. 2020, doi: 10.1016/j.ijheatmasstransfer.2020.120159.

[9] V. Kumar, Vikash, and K.D.P. Nigam, "Multiphase fluid flow and heat transfer characteristics in microchannels," *Chem. Eng. Sci.*, vol. 169, pp. 34–66, Sep. 2017, doi: 10.1016/j.ces.2017.01.018.

[10] Z. Huang *et al.*, "Coupling between an accumulator and a loop in a mechanically pumped carbon dioxide two-phase loop," *Micrograv. Sci. Technol.*, vol. 21, pp. 23–29, 2009.

[11] M. Qingliang, T. Zhang, Y. Feng, Z. Yu, Z. Zhenming, and Z. Zhenhua, "Experimental study on dynamic behavior of mechanically pumped two-phase loop with a novel accumulator in simulated space environment," *Chin. J. Aeronaut.*, vol. 35, no. 12, pp. 102–116, 2022.

[12] J. Wang, B. Yu, C. Qian, J. Shi, and J. Chen, ' 'Experimental study on the boiling heat transfer characteristics of a pump-driven two-phase cooling loop system for high heat flux avionics," *Therm. Sci. Eng. Prog.*, vol. 45, p. 102150, Oct. 2023, doi: 10.1016/j.tsep.2023.102150.

[13] I. Mudawar, "Two-Phase Microchannel Heat Sinks: Theory, Applications, and Limitations," *J. Electron. Packag.*, vol. 133, no. 4, p. 041002, Dec. 2011, doi: 10.1115/1.4005300.

[14] J. Lee and I. Mudawar, "Low-Temperature Two-Phase Microchannel Cooling for High-Heat-Flux Thermal Management of Defense Electronics," *IEEE Trans. Compon. Packaging Technol.*, vol. 32, no. 2, pp. 453–465, Jun. 2009, doi: 10.1109/TCAPT.2008.2005783.

[15] G. Wang, P. Cheng, and A. E. Bergles, "Effects of inlet/outlet configurations on flow boiling instability in parallel microchannels," *Int. J. Heat Mass Transf.*, vol. 51, no. 9, pp. 2267–2281, May 2008, doi: 10.1016/j.ijheatmasstransfer.2007.08.027.

[16] N. Schweizer, P. Stephan, and R. Schlitt, "A Concept for a Miniature, Mechanically Pumped Two-Phase Cooling Loop," *SAE Technical Paper*, 2008-01-1953, 2008, doi: 10.4271/2008-01-1953.

[17] Z. R. Wang *et al.*, "Design and performance of a mechanically pumped two-phase loop to support the evaporation-condensation experiments on the TZ1," *Case Stud. Therm. Eng.*, vol. 10, pp. 650–655, Sep. 2017, doi: 10.1016/j.csite.2017.11.008.

[18] R.V. Bejarano and C. Park, "Active flow control for cold-start performance enhancement of a pump-assisted, capillary-driven, two-phase cooling loop," *Int. J. Heat Mass Transf.*, vol. 78, pp. 408–415, Nov. 2014, doi: 10.1016/j.ijheatmasstransfer.2014.06.069.

[19] M. Crepinsek and C. Park, "Experimental analysis of pump-assisted and capillary-driven dual-evaporators two-phase cooling

loop," *Appl. Therm. Eng.*, vol. 38, pp. 133–142, May 2012, doi: 10.1016/j.applthermaleng.2012.01.022.

[20] J.H. Ambrose, A.R. Feild, and H.R. Holmes, "A pumped heat pipe cold plate for high-flux applications," *Exp. Therm. Fluid Sci.*, vol. 10, no. 2, pp. 156–162, Feb. 1995, doi: 10.1016/0894-1777(94)00092-M.

[21] L. Pereira *et al.*, "A study on the fluid refrigerant charge in a two-phase mechanically pumped loop system using R134a and R1234yf," *Appl. Therm. Eng.*, vol. 158, p. 113727, Jul. 2019, doi: 10.1016/j.applthermaleng.2019.113727.

[22] C. Jiang, W. Liu, Z. Liu, J. Yang, B. Duan, and X. Luo, "Startup characteristics of pump-assisted capillary phase change loop," *Appl. Therm. Eng.*, vol. 126, pp. 1115–1125, Nov. 2017, doi: 10.1016/j.applthermaleng.2017.02.043.

[23] Q. Meng *et al.*, "Experimental study on the transient behaviors of mechanically pumped two-phase loop with a novel accumulator for thermal control of space camera payload," *Appl. Therm. Eng.*, vol. 179, p. 115714, Oct. 2020, doi: 10.1016/j.applthermaleng.2020.115714.

[24] Z. Deng, J. Zhang, Y. Lei, J. Tao, and C. Zhang, "Startup regimes of minichannel evaporator in a mechanically pumped fluid loop," *Int. J. Heat Mass Transf.*, vol. 176, p. 121424, 2021.

[25] J.-X. Wang, Y.-Z. Li, Y. Zhang, J.-X. Li, Y.-F. Mao, and X.-W. Ning, "A hybrid cooling system combining self-adaptive single-phase mechanically pumped fluid loop and gravity-immune two-phase spray module," *Energy Conv. Manag.*, vol. 176, pp. 194–208, Nov. 2018, doi: 10.1016/j.enconman.2018.09.010.

[26] T.D. Swanson and G.C. Birur, "NASA thermal control technologies for robotic spacecraft," *Appl. Therm. Eng.*, vol. 23, no. 9, pp. 1055–1065, Jun. 2003, doi: 10.1016/S1359-4311(03)00036-X.

[27] J. Raetz and J. Dominick, "Space Station external thermal control system design and operational overview," *Epidemiology*, vol. 22, no. 1, p. S146, 1992, doi: 10.1097/01.ede.0000392119.49987.0c.

[28] D. Steiner and J. Taborek, "Flow boiling heat transfer in vertical tubes correlated by an asymptotic model," *Heat transfer engineering*, vol. 13, no. 2, pp. 43–69, 1992, doi: 10.1080/01457639208939774.